H_2 Production in the 440-nm Photodissociation of Glyoxal

L. M. Dobeck,[†] H. M. Lambert,* W. Kong,[‡] P. J. Pisano, and P. L. Houston*

Department of Chemistry and Chemical Biology, Cornell University, Ithaca, New York 14853-1301

Received: July 12, 1999; In Final Form: September 10, 1999

H_2 has been detected following the photolysis of glyoxal at 440 nm using the techniques of vacuum ultraviolet laser-induced fluorescence and (2 + 1) resonance enhanced multiphoton ionization. It is thus confirmed that a fraction of the glyoxal excited at this wavelength dissociates into three photofragments: HCOCOH → H_2 + 2 CO. The most populated vibrational level of those observed was H_2 ($v = 1$), and in this level rotational states from $J = 0-9$ were detected. Doppler profiles of these lines provide estimates of the translational energy and show a **v**||**J** correlation. Of the available energy to the H_2 + 2CO products, 3.1% appears as rotational energy in H_2 ($v = 1$), 17.8% appears as the H_2 ($v = 1$) vibration, and 46.8% appears as H_2 ($v = 1$) translation. Excitation of the 7_0^2 band produces somewhat more of the H_2 + 2CO channel than does excitation of the 0_0^0, 5_0^1, or 8_0^1 bands. These observations are consistent with a model in which trans→cis isomerization precedes dissociation. Rotational excitation with **v**||**J** is caused by the ν_7 torsional motion. The small degree of rotational excitation, the production of H_2 in $v = 1$ and $v = 2$, and the translational energy distribution are all consistent with ab initio calculations of the transition state structure.

I. Introduction

Glyoxal, HCOCOH, has been of interest to spectroscopists and physical chemists since even before the 1970s, when the first analyses of its visible spectrum were made by Ramsay and co-workers.[1−12] In the intervening years a great deal of information has been obtained about both the coupling between the lowest excited singlet state and the lowest triplet state of the molecule[13−20] and about its high-resolution, Doppler-free spectrum.[21] The fluorescence quantum yield for low-lying vibrational levels of the ^1A_u state is on the order of 50%;[22] internal conversion from the S_1 to the S_0 surface is the nonradiative process.[23] Much of the recent interest in this molecule stems from its presence in the polluted tropospheric atmosphere[24,25] and as an intermediate in combustion systems.[26] Its well-characterized spectrum has led to further studies using this molecule to probe collisional energy transfer processes,[27−36] molecular alignment,[37] predissociation of van der Waals complexes,[38−40] and stimulated emission pumping.[39,41,42]

Following the first observations of collisionless predissociation of glyoxal,[43−45] the dissociation dynamics of this molecule have also been examined. The primary dissociation channel appears to be

$$\mathrm{HCOCOH} \rightarrow \mathrm{H_2CO} + \mathrm{CO} \qquad (1)$$

Early observation of H_2 as a final product following photolysis of bulb samples[43−46] showed that there was a noncondensable product other than CO and suggested that another channel might be

$$\mathrm{HCOCOH} \rightarrow \mathrm{H_2} + \mathrm{CO} + \mathrm{CO} \qquad (2)$$

Indeed, detailed theoretical calculations[47−49] have indicated that a transition state to these products occurs on the S_0 surface following rotation of glyoxal about the C−C bond from the ground-state trans conformation to the cis conformation. The dissociation path leading to these three products has been called the "triple whammy channel" (TWC).[47] A comparison of the transition state with the equilibrium *cis*-glyoxal ground state geometry shows that the stationary point has a C−C bond distance of 2.10 Å, about 0.57 Å larger than the equilibrium distance of 1.53 Å. The C−H distances are also increased from 1.10 in *cis*-glyoxal to 1.40 in the transition state. Finally, the change in the H positions relative to each other is dramatic. In *cis*-glyoxal they are 2.46 Å from each other and nonbonding, whereas in the transition state the distance decreases to 1.07 Å, much closer to the equilibrium internuclear distance of 0.741 Å for free H_2. Similar results for the transition state have been calculated recently by Luis Montero and his co-workers at the 6-311G** level.[50] Similar H−H and C−C distances were found for the transition state, which was 2.56 eV higher than the *cis*-glyoxal isomer. The activation energy from the trans isomer is thus 54.5 kcal/mol, similar to that found by the Schafer group at the CCSDT-1 TZ + 2P level.[49]

Further evidence for the triple whammy channel came from the molecular beam photodissociation studies of Hepburn et al.,[51] who examined the arrival time distribution of mass 28 and 30 fragments. Their observations suggested that there were actually three channels to the dissociation. While channel (1) accounted for 65% of the yield and channel (2) accounted for 28%, the remaining 7% was attributed to production of a formaldehyde isomer, thought to be hydroxy methylene

$$\mathrm{HCOCOH} \rightarrow \mathrm{HCOH} + \mathrm{CO} \qquad (3)$$

Burak et al.[52] investigated the photodissociation of glyoxal by monitoring the CO product with vacuum ultraviolet laser-induced fluorescence following dissociation through several vibrational bands of the ^1A_u excited state. Appearance times for the CO were found to be in excellent agreement with the glyoxal

[†] Current address: Institute for Computational Earth System Science, University of California at Santa Barbara, 6487 Calle Real, Unit A, Santa Barbara, CA 93117.

[‡] Current address: Department of Chemistry, Oregon State University, Corvallis, OR 97331.

10.1021/jp992333s CCC: $18.00 © 1999 American Chemical Society
Published on Web 10/22/1999

fluorescence decay times, indicating that there is no long-lived intermediate in the dissociation. The CO was found to be produced almost exclusively in $v = 0$, but the rotational distribution was spread over a very broad distribution peaking at $J \approx 42$. Glyoxal dissociates much more slowly than its rotational period, so it was surprising to find that the Doppler profiles of individual product states showed structural features. Analysis demonstrated that the structure was due to a $\mathbf{v}-\mathbf{J}$ correlation in the products: the CO recoil velocity vector and the CO angular momentum vector are predominantly perpendicular to one another, implying that the dissociation takes place from a planar geometry. Analysis of the joint velocity and rotational distributions suggested that the highest rotational levels of CO are produced in coincidence with the formaldehyde product in channel (1).

Despite the number of studies of this photodissociation system, there has yet to be reported any firm evidence that H_2 is produced in the dissociation, nor has there been any characterization of the H_2 properties that might be compared to those predicted from the calculated transition state geometry. This work was undertaken to detect and characterize the H_2 product, if any, from the reaction.

II. Experimental Section

Jet-cooled glyoxal was excited to selected vibronic bands of the ^1A_u electronic state and the photodissociation products were probed after a delay of 300 ns. Although several detection schemes for probing H_2 were tried, $(2 + 1)$ resonance enhanced multiphoton ionization (REMPI) through the E,F state provided the least interference with other processes and was used in the majority of the work.[53]

Vacuum Chamber. Experiments were performed in a liquid nitrogen cryotrapped, six-way cross vacuum chamber modified by the addition of four extra ports in the horizontal plane and evacuated with an Edwards E2M30-backed Varian VHS-6 diffusion pump. The typical background pressure, as measured by a Granville-Phillips ionization gauge, was 1×10^{-6} Torr, while the average pressure during operation of the molecular beam was 2×10^{-5} Torr. The molecular beam was unskimmed and emanated from a piezoelectric valve[54] with an orifice 500 μm in diameter. The molecular beam, the collinear and counter propagating dissociation and probe laser beams, and direction of light detection by a photomultiplier tube (PMT) were all located in the same plane, as shown in Figure 1. Baffles were inserted in the laser entrance and exit arms of the chamber to reduce scattered light.

Ion Detection. Ion collection was performed using a 1.5 in. diameter focused mesh electron multiplier (Johnston Laboratories) situated $1\ ^1/_4$ in. above the plane of the molecular and laser beams. A grounding plate (2.5 in. diameter) was placed $^7/_8$ in. below the plane of the lasers. A grounded cylindrical shield with 0.5 in. diameter holes spaced at 45° intervals to allow the molecular and laser beams to enter and exit the interaction region served to minimize the perturbation to the electric field caused by the nozzle. The mesh was biased with -3500 V and the output was amplified 25 times by a 300 MHz dc amplifier (Stanford Research Systems model 445).

Although there was no time-of-flight tube or repeller plates, a crude mass resolution was observed and the H_2^+ arrival was well resolved in time from all heavier ions. Since the ion detection mesh was also sensitive to UV photons, the probe laser scattered light signal provided a convenient measure of the zero in arrival time. H^+ and H_2^+ ion peaks with arrival times

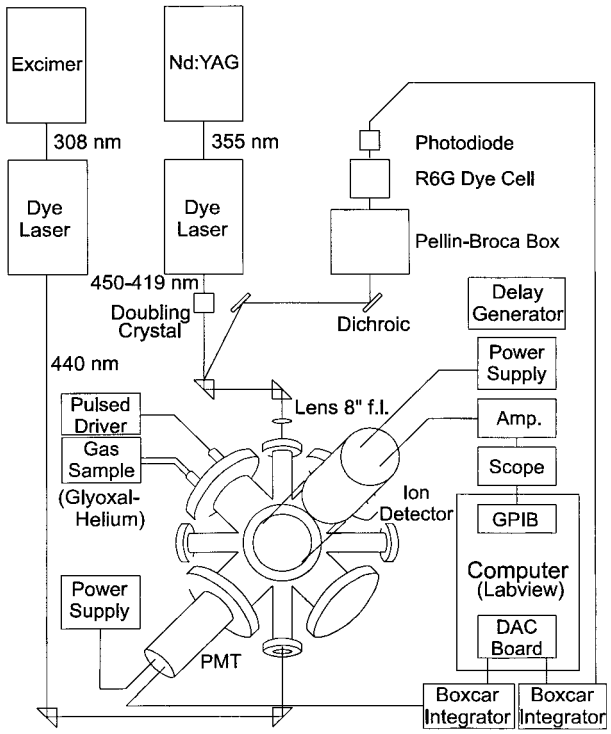

Figure 1. Schematic diagram of the experimental apparatus.

of 100 and 150 ns, respectively, were completely resolved at low signal levels, and only began to overlap at higher signal levels.

The heavier ions were mainly a result of nonresonant ionization of glyoxal by the focused UV probe laser. This mass peak was about 50 times more intense than the H_2^+ ion signal and presented a heavy burden for the ion detector. During the course of these experiments and earlier studies with a Channeltron detector, the useful lifetime of the ion detectors decayed in a nonlinear fashion.

Glyoxal Visible Fluorescence. Glyoxal was dissociated at 440 nm using an excimer pumped dye laser system (Lambda Physik LPX205/FL2002) with pulse energies of 6−12 mJ at 10 Hz. No etalon was used and thus the linewidth was assumed to be that specified by Lambda Physik for their dye laser of 0.2 cm^{-1}. Most work was done exciting glyoxal to the 8_0^1 band in the S_1 manifold. The excitation was partially resolved into rotational branch envelopes. Glyoxal predissociates at this excitation wavelength and fluorescence competes with dissociation. Normalization for fluctuations in photolysis power and pressure variation in gas pulses was performed by monitoring glyoxal fluorescence with a visible PMT (EMI Type 9558QB) and collection lens. An OG515 cutoff filter was placed in front of the PMT to reduce the amount of scattered laser light detected. A power dependence study indicated that the H_2^+ signal from glyoxal photolysis was linear with the dissociation laser power.

Detection of H_2 by VUV LIF. Vacuum ultraviolet laser induced fluorescence (VUV LIF) was explored as a detection scheme for H_2 in preliminary survey work. H_2 ($v = 1$) from glyoxal was probed by LIF using the (3,1) and (2,1) bands of the $B^1\Sigma^+_u \leftarrow X^1\Sigma^+_g$ transition. The 115 nm light was generated by nonresonant tripling in Kr. The UV output from an excimer pumped dye laser system (Lambda Physik LPX 205/FL2002) operating with a *p*-terphenyl/*p*-dioxane solution was focused with a 4 in. focal length lens into the center of a 6 in. long cell containing Kr. The resulting VUV radiation was recollimated

with a 2.75 in. focal length lens which acted as the exit window of the Kr cell and the entrance window of the vacuum chamber. Kr pressures of 50−100 Torr resulted in optimum VUV power over the wavelength range of interest. H_2 ($v = 0$) from glyoxal was also probed by LIF using the (3,0) band and tripling in Xe.

In these experiments, the photolysis and probe lasers intersected at right angles in a mutually orthogonal configuration with the molecular beam. The VUV probe laser light was separated from the UV laser fundamental by use of an evacuated monochromator attached to the probe laser exit arm of the vacuum chamber and was detected by a solar blind PMT with a CsI photocathode. H_2 fluorescence was collected with a lens and detected with a second solar blind PMT placed at 45° to both laser beams. The LIF signal was normalized for the VUV power.

Detection of H_2 by (2 + 1) REMPI. H_2 vibrational and rotational state distributions were obtained using (2 + 1) REMPI through $v' = 0$ in the excited E,F state. H_2 ($v = 1-2$) were probed using the frequency doubled output of a dye laser (Lambda Physik Scanmate 2E, BBO I/II crystals) pumped by the third harmonic of a Nd:YAG laser (Spectra Physics GCR 270) to generate light in the appropriate wavelength range (210−230 nm). The resulting pulse energies of the doubled light were typically between 0.6 and 1.0 mJ. This was well below the level at which Vrakking et al.[55] working in the high probe power regime, observed power broadening with Zeeman and Stark shifts. The probe laser light was focused at the center of the chamber by a MgF_2 lens (focal length 8 in.) positioned before the entrance window.

When probing H_2 ($v = 1$), the fundamental wavelength (ca. 420 nm) was not separated from the doubled light as it was found to have no apparent effect on the results. For H_2 in ($v = 2$), however, the fundamental wavelength (ca. 440 nm) falls within the absorption band of glyoxal. Thus for these experiments, the doubled light was separated from the fundamental light with four Pellin−Broca prisms before exiting the frequency-doubling stage of the dye laser. The polarization of the doubled laser light was horizontal in the laboratory frame and perpendicular to the axis of ion detection.

Relative fluctuations in the doubled light were monitored by sending a reflection from one of the turning prisms that steered the beam to the chamber into a cell filled with a Rhodamine 6G dye solution in methanol. The resulting fluorescence was detected by a fast photodiode (Thorlabs DET200) and the photodiode signal was processed by a gated integrator. Power dependence studies determined that the H_2^+ signal intensity depended on the square of the UV light intensity.

The technique of sum frequency generation (SFG) was used to generate light at the short UV wavelengths (201−205 nm) necessary to detect H_2 ($v = 0$, $J = 0-7$). In this case, the second harmonic of the Nd:YAG laser was used to pump the dye laser which was operated with a Rhodamine 640/methanol dye solution. The visible laser output (40 mJ at 605 nm) was frequency doubled (Lambda Physik BBO III crystal), and the doubled light (10 mJ at 302.5 nm) and residual fundamental light were frequency summed (Lambda Physik BBO II crystal) to generate 0.7 mJ of 201.7 nm light. In order to enhance the SFG process, a quarter wave plate with an antireflection coating centered at 589 nm was placed prior to the first nonlinear crystal. As well, the quartz exit window of the SFG crystal housing was removed in order to reduce absorption losses. The doubled light was removed from the SFG light by using 210 nm dichroic mirrors to steer the laser radiation into the chamber. This reduced the SFG pulse energies by a factor of 5.

For all levels of H_2 probed ($v = 0-2$), the focused probe laser radiation alone produced a background of H_2^+ ion signal. A minor source was the nonresonant ionization of glyoxal and subsequent decomposition. This signal, however, was constant across a scan and simply provided an offset. A more important source, which became apparent when the probe laser frequency was resonant with an H_2 transition to the v and J levels in the E,F state, was due to photolysis of glyoxal at higher energies (shorter wavelengths) than the one photon excitation of glyoxal to the S_1 state. These competing processes were undoubtedly enhanced by focusing the probe laser.

H_2 REMPI transitions in $v = 0$ and $v = 1$ were measured under bulb-like conditions. This served several diagnostic purposes such as finding the line positions and comparing the results obtained by the detection system on a sample with a known distribution. Compressed H_2 effused into the vacuum chamber through a leak valve and a 1 mm diameter tube mounted on one of the arms of the chamber. The chamber was left open to the diffusion pump in order to maintain a pressure below 1×10^{-4} Torr for ion collection.

Data Collection. The experiment was controlled by Labview (National Instruments version 4.0) with the master timings set by a digital delay generator (Stanford Research Systems DG535) which was used to trigger the piezoelectric nozzle power supply, lasers (excimer, Nd:YAG lamps, and Q-switch), data acquisition board (National Instruments Lab PC+ board), and oscilloscope (LeCroy 9450). The H_2 probe laser scanning program was controlled remotely from Labview through a GPIB/RS-232 converter interfaced with the laser's laptop computer. Ion signal data was collected and processed using Labview by downloading (via GPIB) the oscilloscope trace, gating on the signal of interest, and averaging for 30 laser shots. Laser power, monitored for normalization purposes, was collected by the data acquisition board from the output of the gated integrators and also averaged for 30 laser shots.

It was necessary to perform background subtraction because of the large H_2^+ ion signal produced by the probe laser alone. One way in which this subtraction was accomplished was to collect ion signal with the photolysis laser alternately synchronized with the molecular beam or following it by 10 ms every other 30 laser shots. This latter timing was equivalent to doing a one-laser pump−probe experiment with no contribution from 440 nm excitation of glyoxal to the S_1 state. An equivalent configuration allowed the photolysis laser to remain synchronized with the molecular beam, but blocked the photolysis laser with a mechanical shutter every 30 laser shots.

In addition to the wavelength of the probe laser, six channels of data were collected to perform baseline subtraction and to normalize for laser powers. Three quantities, H_2^+ signal, glyoxal fluorescence, and UV power, were collected for the "ON" and "OFF" conditions of the baseline subtraction scheme. ON refers to the two laser pump-probe experiment in which the photolysis laser intersected the molecular beam 300 ns before the probe laser, whereas OFF refers to the one laser experiment in which only the probe laser intersected the molecular beam. As the probe laser was always ON, the ON and OFF channels for the probe laser monitor were equivalent. Taking the difference between the ON and OFF channels for both the H_2^+ signal and the glyoxal fluorescence removed the background for these quantities. In the following sections, dissociation of glyoxal at

the UV probe laser wavelengths refers to the OFF signal, while dissociation of glyoxal at 440 nm refers to the difference signal ON − OFF.

PHOFEX Spectrum. Photofragment excitation (PHOFEX) spectra were obtained by fixing the probe laser wavelength on an H_2 REMPI transition (out of $v = 1$, $J = 1$) and monitoring the H_2^+ ion signal while the photolysis laser wavelength was scanned from 438 to 457 nm. The absorption spectrum of glyoxal has well-resolved vibronic bands in this region. Fluorescence from excited glyoxal was simultaneously detected by means of a PMT. Two cutoff filters (GG395 and GG400) were placed before the PMT to reduce the level of scattered laser light detected.

Glyoxal Preparation. Monomeric glyoxal was prepared by pyrolyzing the trimeric dihydrate precursor (Aldrich) in a glass vacuum line. The trimer was heated to 150 °C in the presence of excess phosphorus pentoxide until the evolution of CO occurred, at which point the heating source was turned off. After the pressure evolution subsided, the mixture was heated to 220 °C. The glyoxal monomer was given off from the black tarry reaction mixture as a yellowish green gas and was collected in a liquid nitrogen cooled trap after passing through two traps cooled with salt/ice baths to remove water vapor. As formaldehyde, a major byproduct, also collects in the liquid nitrogen cooled trap, it was necessary to perform a final trap to trap distillation with a dry ice/acetone bath to allow most of the formaldehyde to be removed while retaining the glyoxal. Several freeze−pump−thaw cycles were carried out to eliminate CO and other impurities trapped in the solid glyoxal lattice. Long term storage (2 months) at liquid nitrogen temperatures maintained the sample integrity but with prolonged exposure to near ambient temperatures, polymerization to a white solid occurred on the time scale of a few days.

To entrain the glyoxal monomer in a molecular beam, He was allowed to flow through the trap containing the glyoxal sample in the ice/water bath at a backing pressure of about 600 Torr. The vapor pressure of glyoxal at 0 °C is about 52 Torr giving a beam of approximately 8% glyoxal in helium.

The presence of formaldehyde in our glyoxal sample was established by comparing spectra obtained in separate LIF experiments with glyoxal and formaldehyde. Wavelengths for excitation of (353 nm) and observation of fluorescence (412 nm) from formaldehyde were selected in spectral regions in which glyoxal did not absorb or fluoresce. The resulting spectra were nearly identical.

III. Results

H_2 was detected following the photodissociation of glyoxal both using VUV laser induced fluorescence through the $B^1\Sigma^+_u \leftarrow X^1\Sigma^+_g$ transition and using REMPI through the E,F state. Figure 2 shows the LIF spectrum of H_2 and CO produced in the photodissociation of glyoxal on the 8_0^1 band. The stronger lines identified in this figure are the hydrogen transitions, while the weaker and more closely spaced lines are due to laser excitation of CO transitions.

Because formaldehyde also dissociates to products H_2 and CO at wavelengths below about 357 nm, the choice of photolysis and detection laser wavelengths was an important factor in determining that photodissociation of glyoxal was indeed the source of the observed H_2. One reason for abandoning the VUV LIF detection scheme described in the previous section was that the UV laser light (330−345 nm) required to frequency triple in the rare gases also passed through the chamber and fell within the absorption band of formaldehyde (250−360 nm). The (2 + 1) REMPI scheme for detecting H_2 ($v = 1-2$), however, involved laser wavelengths which fell outside the region of formaldehyde absorption. The exception was the SFG technique for detecting H_2 ($v = 0$) in which light at 302.5 nm was present, but this was largely removed by using dichroic mirrors (210 nm) to send the probe laser light into the chamber. A diagnostic experiment revealed that although H_2 could be clearly detected when formaldehyde was dissociated at 353 nm, the same REMPI detection system was unable to detect H_2 when the photolysis wavelength was switched to 440 nm as used in the glyoxal experiments. This test shows that the wavelengths used for probing and detection of H_2 from glyoxal do not produce H_2 from ground-state formaldehyde.

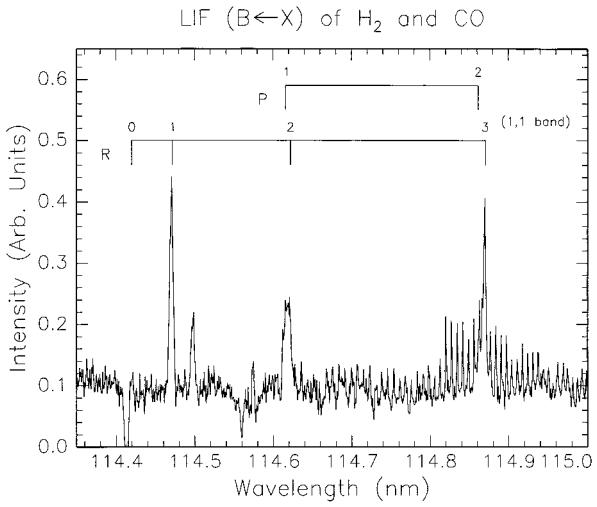

Figure 2. Laser-induced fluorescence spectrum of H_2 and CO produced in the photodissociation of glyoxal.

REMPI signals from H_2 were observed in the presence of both the dissociation laser and the probe laser and also in the presence of the probe laser alone. The data acquisition method described in the previous section allowed us to separate the two contributions by a simple subtraction routine. Thus all results given here for the 440 nm photodissociation have had the one laser signal removed. Power dependence studies for the 440 nm photolysis showed that both the glyoxal fluorescence and the H_2 signal were linear in the 440 nm laser power. The H_2 signal was shown to be nearly quadratic in the probe laser intensity, as a slope of 1.9 ± 0.1 was obtained from the plot of the log of integrated ion signal vs the log of the UV probe laser monitor. With the same probe laser powers, but with pure H_2 under bulb-like conditions, the slope was found to be 1.85 ± 0.07. These values for the slopes are consistent with the (2 + 1) REMPI detection scheme in which the two photon absorption to the E,F state is followed by a saturated ionization step.[56]

H_2 signals from the probe laser alone arise from glyoxal dissociation at different wavelengths depending on the quantum state of the H_2 detected. Wavelengths for Q(1) transitions, for instance, are 201.78 nm for $v = 0$, 210.61 nm for $v = 1$, and 219.68 nm for $v = 2$. Power dependence studies also showed a variation with wavelength. The slopes obtained from plots of the log of integrated ion signal vs the log of laser power for H_2 ($v = 1$, $J = 1$) and H_2 ($v = 2$, $J = 3$) were 2.01 ± 0.09 and 2.5 ± 0.2, respectively. It is not clear at this point whether these one laser signals were due to single UV photon dissociation of glyoxal or due to a multiphoton process. In this spectral region the absorption by glyoxal is weak, lying between the diffuse B−X bands (320−230 nm) and the stronger C−X bands (205−185 nm). Unlike the photolysis at 440 nm, no fluorescence is

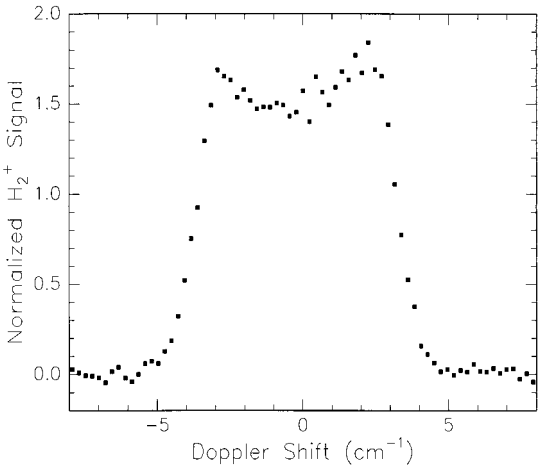

Figure 3. Doppler line shape of H_2 ($v = 1$, $J = 1$) following photodissociation of glyoxal at 440 nm.

observed, indicating a more direct dissociation through higher energy states of glyoxal accessible at the UV wavelengths.

The shapes of Doppler profiles are generally sensitive to $\boldsymbol{\mu}-\mathbf{v}-\mathbf{J}$ vector correlations, where $\boldsymbol{\mu}$ refers to the transition dipole moment of the absorbing parent molecule, and **v** and **J** refer to the photofragment velocity and angular momentum vectors, respectively. However, for glyoxal, the rotational period is much shorter than the predissociation timescale, and consequently, the "memory" of the absorption is lost due to the rotations so that any $\boldsymbol{\mu}-\mathbf{v}$ or $\boldsymbol{\mu}-\mathbf{J}$ correlations are washed out. However, the $\mathbf{v}-\mathbf{J}$ correlation is caused by the breakup of the transition state and the interactions between the photofragments as they separate, and it will contribute to the Doppler line shape regardless of the parent rotation. Figure 3 displays the normalized Doppler profile of the H_2 ($v = 1$) Q(1) REMPI signal following dissociation of glyoxal at 440 nm. All H_2 ($v = 1$, $J = 1-5$) Doppler line shapes recorded for the 440 nm photolysis of glyoxal appear to be generally flat-topped with a reproducible dip at line center. The slight dip observed in the Doppler profiles indicates that there is a measurable $\mathbf{v}-\mathbf{J}$ vector correlation. Unambiguous determination of the vector information requires probing the rotational level in different branches, but unfortunately, the other branches (O and S) in the two-photon detection scheme employed here are less intense by a factor of 50.

Care was taken to minimize any bias in the detection step since hypothetical fly-out of H_2 in a direction transverse to the laser beam propagation axis could also cause a dip in the Doppler profile at line center. The photolysis laser beam diameter was about 3 mm and much larger than the focused probe laser beam diameter of less than 0.5 mm. As glyoxal was dissociated in a bigger volume than that probed, fly-out of H_2 from the probe beam was balanced by fly-in of H_2 from the larger surrounding volume of the photolysis beam. The time for fly-out was also investigated by varying the delay between the photolysis and the probe laser. Doppler profiles were recorded for a range of delay times from 50 ns to 1 μs. The appearance of the dip at line center relative to the wings of the Doppler profile was not noticeably affected by the delay time over the range 200−500 ns. At shorter and longer delay times the overall signal intensity and hence signal-to-noise ratio dropped below that which allowed for useful comparisons of dip to wing intensities. However, it appears that fly-out was not a serious problem at the 300 ns delay time used, and hence was not the cause of the observed dip at line center in the Doppler profiles.

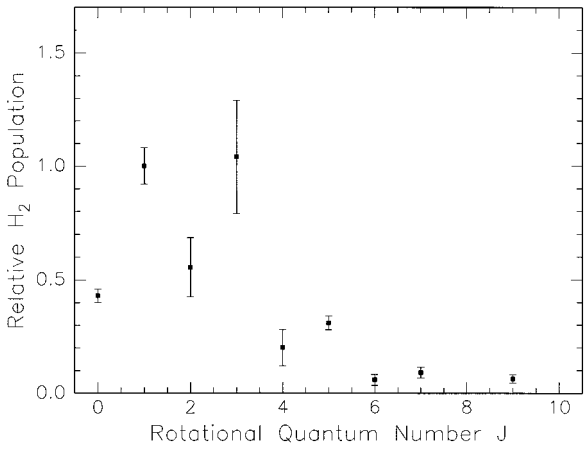

Figure 4. H_2 ($v = 1$) rotational distribution following photodissociation of glyoxal at 440 nm.

Information about the energy partitioning between rotation and translation is obtained from the widths of the Doppler profiles. Diagnostic experiments have determined that the widths of the rotational lines are not affected by space charge broadening at the typical laser pulse energies of 0.6 mJ and gas pressures of less than 4×10^{-5} Torr (8% glyoxal/helium), and that the effective VUV bandwidth of the laser (Gaussian lineshape function with full width at half maximum = 0.46 ± 0.02 cm^{-1}) is a small fraction of the total line width. From a comparison of several (3−9) profiles obtained for each *J*, it appears that the widths are independent of *J*, having an average value of 7.28 ± 0.26 cm^{-1} (full width half maximum). Widths for low and high *J* of H_2 ($v = 1,2$) lines obtained in the UV photolyses of glyoxal at 210 and 220 nm also appeared to be the same within their uncertainties, with values near 9 cm^{-1} for $v = 1$ and 8 cm^{-1} for $v = 2$.

Distributions of relative population in rotational states have been obtained for H_2 ($v = 1$) for both 440 nm photolysis and UV photolysis (around 210 nm) (see Figures 4 and 5). The H_2^+ ion signals were normalized for variations in the detection laser power (quadratic dependence) and in the glyoxal pressure and photolysis laser power and then integrated to obtain intensities. Due to the degradation of the detector mesh sensitivity during an experiment, a reference line was recorded every other scan. Relative ion intensities were derived by normalizing by the average of the reference line intensities taken before and after the line of interest. As two dyes were required to span the spectrum from low to high *J*, two different reference lines were used: $J = 1$ for low *J* and $J = 7$ for high *J*. The two segments of the distribution were knit together using lines common to both dye tuning curves ($J = 5-7$). Relative populations were obtained by dividing the normalized ion intensities by the two-photon transition probabilities calculated for the (2 + 1) REMPI scheme used here.[57] The error bars in Figures 4 and 5 are estimates of ±1 standard deviation from the average of 3−10 normalized data sets for each *J*. The error bar for the $J = 1$ reference line was estimated from replicate scans over the line after correcting the intensities for a linear decay with time. High *J* lines had proportionately higher error bars due to the very low signal-to-noise levels and the uncertainty in the normalization factors for the different reference lines.

Weighted linear least square fits to plots of the natural logarithm of the rotational population divided by the rotational and nuclear spin degeneracies vs the rotational energy yielded rotational temperatures as fitting parameters. In the case of the UV photolysis, all of the data were well represented by a rotational temperature of 2215 ± 33 K. For the photolysis at

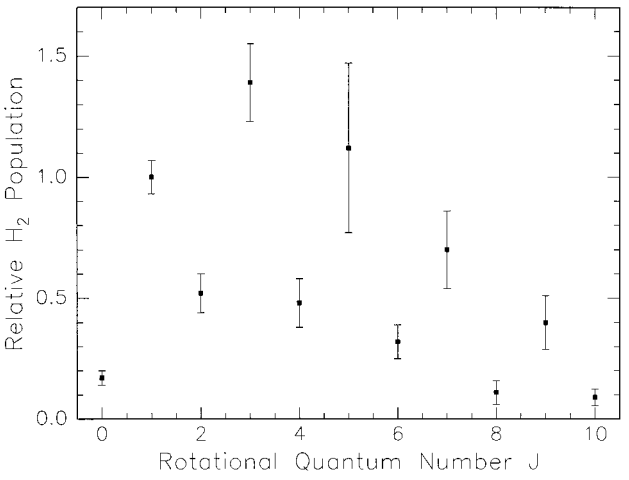

Figure 5. Rotational distribution of H_2 ($v = 1$) following dissociation of glyoxal at ca. 210 nm.

440 nm, however, a rotational temperature of 800 ± 23 K only fitted well the $J = 0-7$ data. An average rotational energy for all of the data ($J = 0-9$) of 725 ± 52 cm^{-1} was calculated by weighting the rotational energies by the population in each level.

The H_2 ($v = 0$) REMPI signal was not observed in the photolysis of glyoxal at 440 nm, and only the signal from ($v = 0$, $J = 1$) was detected in the UV photolysis. This was likely due to the fact that our overall efficiency for detection of $v = 0$ was a factor of about 65 less than for $v = 1$ detection. The REMPI scheme itself is a factor of 2.6 less sensitive for detecting H_2 ($v = 0$) than for $v = 1$.[57] Since the REMPI signals scaled with the square of the probe laser power, the five times weaker probe laser power at 202 nm compared to 210 nm resulted in a loss of a factor of 25 in sensitivity. With signal-to-noise ratios typical of the H_2 ($v = 1$, $J = 1$) scans, we estimate that H_2 ($v = 0$) signals could be detected with a loss of up to a factor of 10 in sensitivity. This leads to an upper limit on the ratio of vibrational populations for $v = 0$ and $v = 1$, that is, $P(v = 0)/P(v = 1) \leq 6.5$.

Preliminary scans of higher vibrational states ($v = 2-3$) have revealed population in rotational levels up to $J = 9$ in the case of the UV photolysis and somewhat colder distributions from the 440 nm photolysis. Our mesh detector failed before we finished taking scans complete with laser powers and glyoxal pressure monitors. Fully normalized $v = 2$ distributions were obtained with the detector in its last stages of usefulness, and hence with less than optimal signal-to-noise ratios. Nevertheless, it was clear that in going from $v = 1$ to $v = 2$, the population from the 440 nm photolysis dropped off more rapidly (a factor of 2−3) than from the UV photolysis. This resulted in a much smaller difference between the signals obtained with both lasers firing and with the probe laser alone. The $v = 2$ rotational distribution from the UV photolysis was determined, but that from the 440 nm photolysis was too noisy to obtain reliable relative populations. Although odd J states (those with the higher nuclear spin statistical weight) up to $J = 7$ were observed, only the $J = 3$ signal had a signal to noise ratio greater than unity. The REMPI calibration factors for relating ion intensities to populations are very nearly the same for $v = 2$ (2.3) and $v = 1$ (2.6),[57] so that the observed factor of 2−3 drop in relative ion signals for $v = 2$ compared to $v = 1$ does give a crude estimate of the relative vibrational population for H_2 produced in the 440 nm photolysis of glyoxal.

The partitioning of the available energy among the three products of the triple whammy channel is summarized in Table 1. The available energy of ∼67 kcal mol^{-1} was calculated as the difference between the 440 nm photon energy and the −2 kcal mol^{-1} heat of reaction.[51] The internal energy of the jet-cooled glyoxal was assumed to be negligible. Notice that the partitioning among the H_2 degrees of freedom only considers the first vibrationally excited level ($v = 1$). This vibrational energy amounts to ∼12 kcal mol^{-1} or 18% of the available energy. The average H_2 ($v = 1$) translational energies determined from the Doppler widths for $J = 0$ to 5 were not noticeably different. The available energy partitioned into H_2 translation was therefore estimated as the average translational energy for the combined $J = 0-5$ data sets, which amounted to 47% or ∼31 kcal mol^{-1}. The energy disposal into H_2 rotation is small, amounting to about 2 kcal mol^{-1} or 3% of the available energy. H_2 thus takes up about 68% of the available energy leaving 32% (∼21 kcal mol^{-1}) to be partitioned among the internal and translational energies of the two CO coproducts.

TABLE 1: Average Partitioning of Available Energy among Products in the Triple Whammy Channel

product	mode	energy disposal (cm^{-1})	% available energy[a]	ref
H_2 ($v = 1$)	rotation	725 ± 52	3.1	this work
	vibration	4161	17.8	this work
	translation	10970 ± 880	46.8	this work
2CO	translation + internal	7574	32.3	this work
	translation	5246	22.4	51
	rotation	2328	9.9	51,[b] this work
	vibration	0	0.0	52

[a] Available energy = $E_{h\nu}$(440 nm) − $\Delta H_{reaction}$ = 23430 cm^{-1}. [b] $E_{trans+int}$ (2CO) − E_{trans}(2CO).

The effect of parent vibration on the photofragmentation yield was investigated in a PHOFEX experiment. With the probe laser wavelength fixed to detect H_2 ($v = 1$, $J = 1$), the dissociation laser wavelength was scanned from 438 to 457 nm. Five different vibrational bands in S_1 glyoxal were excited: the 0_0^0 origin band near 455 nm, the 7_0^2 band near 445.6 nm (torsional motion about the C−C bond), the 5_0^1 band near 444.5 nm (the in-plane C−C−O bend), the weak $12_0^1\ 7_0^1$ band near 442.5 nm (combination band of C−C−O bending and C−C torsional motion), and the 8_0^1 band near 440 nm (out of plane C−H wag).

Both the H_2^+ ion signal generated by the REMPI probe laser and the glyoxal fluorescence signal generated by the photolysis laser were recorded. The spectra displayed in Figure 6 are the result of averaging three data sets and have been scaled to give the same intensity of the 0_0^0 origin band and displaced vertically relative to one another for clarity. The peaks are due solely to the photodissociation of glyoxal by the photolysis laser while dissociation by the UV probe laser contributes only to the baseline.

The laser powers were not monitored directly in this experiment. It is likely that the photolysis laser energy dropped off at the long wavelength end of the scan as our apparent ratio of fluorescence intensities for the 0_0^0 and 8_0^1 bands is a factor of 2−3 less than reported elsewhere.[52,58] However, the ratio of PHOFEX signal to fluorescence signal is independent of the photolysis laser energy as the measured linear dependences of both signals cancel. The stability of the probe laser energy, on the other hand, is readily apparent in the appearance of the baseline in the PHOFEX spectrum. Recall that there is a substantial H_2 signal due to the probe laser alone interacting with glyoxal. With the probe laser fixed in wavelength on an H_2 REMPI transition, the resulting resonant signal provides a background or baseline for the experiment which is highly

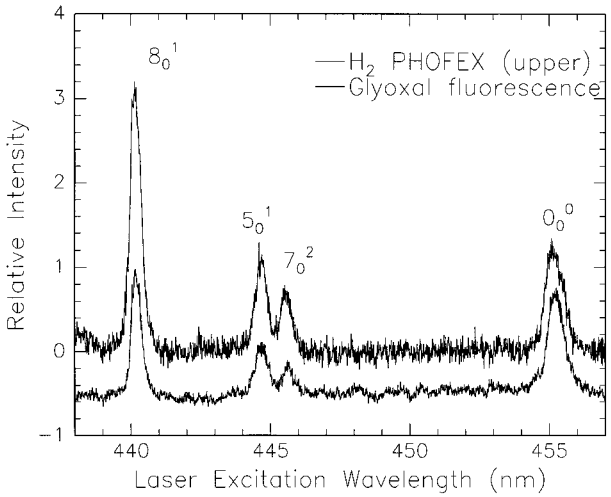

Figure 6. Glyoxal photofragment excitation spectrum for H_2 ($v = 1$, $J = 1$) (upper) and laser-induced fluorescence spectrum (lower).

sensitive (nonlinear dependence) to variations in the probe laser energy. The flat baseline in the PHOFEX spectrum indicates that there was no long term drift in probe laser frequency or energy.

IV. Discussion

A. H_2 as Primary Photoproduct. H_2 has been detected following the photolysis of glyoxal at 440 nm using the techniques of VUV-LIF and (2 + 1) REMPI. The VUV-LIF method was eventually abandoned in favor of detection by the REMPI scheme for several reasons. Due to the extensive nature of the H_2 spectrum with its well separated rovibrational level spacings, the narrow tuning range of the VUV-LIF technique made it unsuitable to determine H_2 product state distributions. More importantly, the frequency tripling scheme used to generate tunable VUV radiation to detect H_2 by LIF exposes the chamber to UV light at wavelengths shorter than the threshold to produce H_2 from the photolysis of formaldehyde. Since formaldehyde is present both as a contaminant from the synthesis of glyoxal and as a primary photoproduct from the photolysis of glyoxal, it was deemed prudent to use a detection scheme which avoided laser wavelengths which could produce H_2 from a source other than the photolysis of glyoxal. It was clearly demonstrated in diagnostic experiments with formaldehyde that the REMPI detection scheme detected H_2 only when the photolysis laser was tuned to a formaldehyde absorption feature (353 nm) but not when the photolysis laser was tuned to a glyoxal absorption (440 nm).

The above diagnostic experiments only discriminate against absorption by cold, ground state formaldehyde which is present in the beam as a contaminant. However, formaldehyde is also present as a major product of glyoxal photodissociation. The energy available to the product formaldehyde internal energy, although well below the threshold for unimolecular dissociation to CO and H_2, is not negligible. In molecular beam studies of the photolysis of glyoxal at 440 nm, Hepburn et al.[51] have determined that an average of 15 000 cm^{-1} is deposited into vibration and rotation of the formaldehyde product. As a result, the absorption spectrum of these hot formaldehyde products may be sufficiently shifted relative to the ground state into regions where the photolysis or probe laser light may be absorbed and effect dissociation.

For the triple whammy channel, a single 440 nm photolysis laser photon is absorbed by glyoxal and the resulting H_2 product absorbs three 210 nm probe laser photons in the (2 + 1) REMPI detection scheme. For the hypothetical scenario of the secondary photolysis of hot formaldehyde, glyoxal is dissociated by 440 nm light to produce rovibrationally excited formaldehyde which either absorbs a second 440 nm photon (within the laser pulse) or a 210 nm probe laser photon and dissociates to H_2 and CO. The H_2 is detected by absorbing three probe laser photons in the (2 + 1) REMPI scheme. Power dependence studies of the observed H_2 signal obtained from the 440 nm photolysis of glyoxal reveal a linear dependence on the photolysis laser and a quadratic dependence on the probe laser. The quadratic dependence on the probe laser power was also found in bulb studies with pure H_2. These results are consistent with the triple whammy channel if the absorption of the third probe laser photon is saturated as is typical of the ionization step in (2 + 1) REMPI detection schemes.

The power dependence studies could be viewed to be consistent with the secondary photolysis scenario only if either the dissociation of the hot formaldehyde within the photolysis laser pulse is saturated, or if two absorption steps in the four photon process within the probe laser pulse duration (dissociation of the hot formaldehyde and detection of the H_2 product) are saturated. Given that the photolysis laser was not focused and that the signal was linear over an order of magnitude change in the laser power, it is highly unlikely that an absorption by hot formaldehyde of a second 440 nm photolysis laser photon would be so strong as to fully saturate the transition. Due to the focused nature of the probe laser, however, we cannot rule out completely the occurrence of a saturated absorption of the probe laser by hot formaldehyde from the results of the power dependence studies. The H_2 signal from the photolysis of glyoxal by the probe laser alone, for instance, also exhibits a near quadratic power dependence, despite being at least a four photon process.

Consideration of the widths of the H_2 Doppler profiles makes it clear that the observed H_2 signals do have their origin with the triple whammy channel. The energy available for disposal into the H_2 product from the secondary photolysis of hot formaldehyde at 440 nm or 210 nm is much greater than from the triple whammy channel. Using the conservation of energy and linear momentum, the maximum Doppler widths for H_2 ($v = 1$, $J = 1$) can be calculated for the two hypothetical scenarios of secondary photolysis of hot formaldehyde at 440 nm and 210 nm as 12 and 16 cm^{-1}, respectively. These calculated widths are upper limits and assume that the accompanying CO has no internal energy, that is, that the coproducts are CO ($v = 0$, $J = 0$). Calculation of the partitioning of the translational energy among the three product molecules in the triple whammy channel requires the geometry of the transition state to be known and will be discussed below. Nevertheless, it is evident that the energy available for H_2 translational energy from the hypothetical photolysis of hot formaldehyde would produce Doppler widths much in excess of what has been determined by experiment (see Figure 3), and with less available energy, the triple whammy channel provides a closer match with experiment.

REMPI signals for H_2 ($v = 0-2$) have been observed after dissociation of glyoxal at UV wavelengths near 201, 210, and 220 nm with the focused probe laser. These signals were observed to have a higher power dependence than the two-laser pump-probe experiments with dissociation at 440 nm. It is not clear whether the one laser signals resulted from a partially saturated single-photon dissociation or were due to a multiphoton dissociation process. The absorption spectrum of glyoxal

in this region lies between the diffuse B−X (320−230 nm) bands and the stronger C−X (205−185 nm) bands. No fluorescence accompanied the H_2 REMPI signals, unlike the visible dissociation at 440 nm, indicating that the UV photolysis accessed higher electronic states of glyoxal. Energy partitioning in this process resulted in greater H_2 rotation, vibration, and translation than observed for the 440 nm photolysis, in keeping with the larger available energy. Overall signal levels for H_2 ($v = 1$) from the UV photolysis were comparable to or greater than those observed in the visible photodissociation.

B. Planar Dissociation Model. Theoretical calculations by Osamura et al.[47] have determined an approximate transition state for the triple whammy channel by constraining the symmetry to C_{2v} as reactant (*cis*-glyoxal) separates into products (H_2 + 2CO), thereby conserving orbital symmetries. The predicted planar structure of the stationary point has an imaginary frequency (2161*i*) for the in plane symmetric stretch normal mode which leads to products. It is not a true transition state because there is a second imaginary frequency (96*i*) which corresponds to an out of plane bending vibration. The extremely low magnitude of the out of plane imaginary frequency suggests that the true nonplanar transition state is well approximated in energy and geometry by that predicted with the constraint to C_{2v} symmetry.

The partitioning of translational energy among the three product molecules of the triple whammy channel has been modeled assuming a symmetrical, planar geometry of breakup and further that the CO molecules take up identical internal and translational energies. The recoil axes of the three products define a Y shape with the H_2 pushing off against the center of mass of the two CO molecules. The CO molecules recoil along the arms of the Y at an angle of separation of 123° as found in the normal mode leading to products. Considering only the components of momentum along the axis of H_2 recoil, the H_2 LAB frame kinetic energy release, KE(H_2), is related to the relative translational energy in the center of mass frame, E_{trans}(rel), as follows

$$\mathrm{KE(H_2)} = E_{trans}(\mathrm{rel})\frac{m(\mathrm{H_2C_2O_2})/(2m(\mathrm{CO}))}{[1 + m(\mathrm{H_2})/(m(\mathrm{CO})\cos(\theta/2))]^2} \quad (4)$$

where $m(\ )$ refers to the masses of the indicated molecules, θ is the angle of separation between the CO recoil directions, and $E_{trans}(\mathrm{rel}) = {}^1/_2\,\mu_{H_2-C_2O_2}\,(\mathbf{v}_{H_2} - \mathbf{v}_{CO} - \mathbf{v}_{CO})^2$

The H_2 kinetic energy release predicted by this simple model behaves well in the two hypothetical limits when the angle between the CO molecules is 180° or 0°. In the limit when $\theta =$ 180° and the CO molecules depart leaving a stationary H_2, eq 4 predicts zero kinetic energy release for H_2. In the even less realistic limit when $\theta = 0°$ and the two CO molecules leave together along the same line, the model predicts that the H_2 gets 90% of the relative translational energy. This is close to that expected (96%) for separation of two structureless particles of mass 2 (H_2) and 56 (C_2O_2).

In the normal mode calculated by Osamura et al.[47] to lead to products in the triple whammy channel, the angle of separation between the two CO molecules was 123°. With this angle, eq 4 predicts that the H_2 receives about 78% of the energy available for translation. For H_2 ($v = 1$, $J = 1$) accompanying two molecules of CO ($v = 0$, $J = 0$), the maximum Doppler width would be 8.5 cm^{-1}. This agrees well with the experimental value of the full width measured near the baseline of 8.6 ± 0.2 cm^{-1} and provides further support that the observed H_2 does indeed come from the triple whammy channel and not from secondary photolysis of hot formaldehyde produced in channel (1).

CO translational energies can likewise be predicted using eq 4. For CO ($v = 0$, $J = 0$) accompanying H_2 ($v = 0$, $J = 0$) or H_2 ($v = 1$, $J = 1$), the translational energies are about 2550 or 2090 cm^{-1}, respectively. These predictions of CO translational energies are within the range of values obtained by extrapolating the CO linewidth measurements in the glyoxal photodissociation work of Burak et al.[52] to $J = 0$, and correspond to velocities of 1480 and 1340 ms^{-1}, respectively. These CO model results are also consistent with the molecular beam work of Hepburn et al.,[51] which showed that the CO translational energy distribution inferred for the triple whammy channel peaked around 7 kcal mol^{-1} with a fwhm of 7 kcal mol^{-1}, giving velocities in the range 1450 ± 370 ms^{-1}.

The consistency of the agreement of experimentally observed translational energies with those predicted by making use of the theoretical calculations is encouraging. Further support of the theoretical results is apparent from the approximate vibrational distribution we obtained for the H_2 product, which shows significant population at $v = 1$. The H−H bond length in the constrained geometry of the approximate transition state was determined to be 1.093 Å.[47] This is much greater than the equilibrium bond length of 0.741 Å for free H_2 in its ground vibrational state. When breakup of the transition state occurs leading to products, the stretched H−H bond should lead to vibrationally excited H_2. The 1.093 Å H−H bond length determined for the approximate transition state falls between the maximum bond extensions obtained from the potential energy curve for the H_2 electronic ground state for $v = 1$ (1.013 Å) and $v = 2$ (1.120 Å).[59] Thus the theoretical calculations of the approximate transition state geometry for the triple whammy channel dissociation of glyoxal predict a vibrational distribution for the H_2 product with significant excitation in $v = 1$ or 2, in qualitative agreement with experiment.

C. Energy Partitioning in the Triple Whammy Channel. In Table 1, the average energy disposal in the two CO molecules is listed as 32%, estimated from the leftover energy after accounting for the disposal into H_2 ($v = 1$) as the other product. From information learned in earlier studies, the partitioning of this energy into internal and translational degrees of freedom can be determined. Burak et al.[52] did not observe any vibrationally excited CO in their experiments, so the internal energy must be rotational. Hepburn et al.[51] inferred a maximum of 15 kcal mol^{-1} in translational energy for both CO molecules which accounts for 22% of the available energy, leaving 10% in CO rotation. The CO translational energy distribution featured a fairly broad peak around 7 kcal mol^{-1} indicating that equal sharing between the two CO molecules was the most probable situation. If the rotational energy disposal is also symmetrical, then $J = 24$ is the highest rotational state that could be populated simultaneously in both CO molecules. With unequal sharing of rotational energy, the maximum rotational state to be populated by one CO would be $J = 34$. This agrees well with the earlier conclusion that the triple whammy channel contribution to the total CO rotational distribution from the photolysis of glyoxal at 440 nm was limited to lower J than the bulk of the distribution (peak at $J = 42$).[52]

The total energy found in translation for the three products is about 69% of the available energy, or 46 kcal mol^{-1}. This value is close to the large activation energy determined for the triple whammy channel both experimentally (47 kcal mol^{-1})[60] and by ab initio theoretical calculations (54.5−54.6 kcal mol^{-1}).[49,50] The triple whammy channel is slightly exothermic so that the energy of activation is released to the products. Because the approximate transition state calculated in C_{2v}

symmetry is characterized by bond lengths more typical of the products H_2 ($v = 1$) and CO ($v = 0$) than to the reactant *cis*-glyoxal, it appears that the activation barrier is late along the dissociation pathway. The energy of the activation barrier would be released on breakup of such a transition state mainly in the form of kinetic energy of separation between the products, as observed.

H_2 rotation cannot arise from a purely planar, symmetric, and concerted dissociation process as indicated by the approximate transition state of Osamura et al.[47] It requires an out of plane motion or an asymmetry in the planar dissociation. The torsional motion about the C−C bond in glyoxal is such an out of plane motion and effects the necessary trans to cis isomerization of glyoxal on the pathway from reactant to transition state in the triple whammy channel. The symmetry elements of the torsional modes in *cis*- and *trans*-glyoxal are correlated with the out of plane normal mode in the constrained C_{2v} stationary state. It is this mode which has the second imaginary frequency (in addition to that of the reaction coordinate), thereby indicating that the true transition state for the triple whammy channel must be slightly nonplanar. If the product H_2 rotation were to have its origin in this out of plane motion, then the partitioned energy should be on the order of the trans−cis energy difference. The experimental[3,61] (1125 ± 200 cm^{-1}, 1350 ± 200 cm^{-1}) and theoretical[49] (1490 cm^{-1}) values for this energy difference are within a factor of two of the average rotational energy determined for H_2 ($v = 1$) of 725 ± 52 cm^{-1}.

D. Vector Correlation (v−J) for H_2. The origin of the H_2 rotational motion can be better understood with information obtained from the **v**−**J** vector correlation. This vector property is a measure of any correlation in the spatial distribution of the photofragment velocity and angular momentum vectors. Such an effect arises in the exit channel of the potential energy surface as a result of interactions between the separating photofragments. The dissociation mechanisms leading to H_2 rotation, mentioned in the previous section, predict opposite **v**−**J** correlations. If the breakup of the planar transition state occurred asymmetrically, with the two CO fragments unequally pushing off from the H_2, then the resulting torque would spin the H_2 in the plane of dissociation. In this situation, the velocity of recoil would be perpendicular to the angular momentum vector and the H_2 rotation would be frisbee-like. Out of plane motion in the transition state, such as torsional motion about the C−C bond, on the other hand, would lead to propellor-like H_2 rotation upon dissociation, with the recoil velocity parallel to the angular momentum.

Although the slight dip observed in the Doppler profiles indicates that there is a measurable **v**−**J** vector correlation, understanding the polarization dependence of the probed ($E,F^1\Sigma_g^+ \leftarrow\leftarrow X^1\Sigma_g^+$) Q branch transitions is not a trivial task. As noted by Kummel, Sitz, and Zare,[62] one must account for both two-photon transition paths ($\Sigma\leftarrow\Pi\leftarrow\Sigma$ and $\Sigma\leftarrow\Sigma\leftarrow\Sigma$) when calculating the polarization dependent line strength factors, $P_0^{(2)}/P_0^{(0)}$. As shown by Hanisco and Kummel,[63] the ratio of these paths is related to the ratio of intensities of Q vs O,S branches and can be used to calculate two unique values for $P_0^{(2)}/P_0^{(0)}$. Using the measured ratio for the Q to S branch transitions,[56] we calculate the $P_0^{(2)}/P_0^{(0)}$ values for the Q(1) transition to be −0.06 ($\epsilon_{probe}\perp\mathbf{J}$) or 0.4 ($\epsilon_{probe}||\mathbf{J}$). We use the small negative value ($P_0^{(2)}/P_0^{(0)} = -0.06$) as the real polarization dependent line strength factor because its magnitude and sign are consistent with other experimental observations of H_2 alignment.[64] Assuming a perfect **v**⊥**J** correlation, one would measure a Doppler profile with more intensity in the center ($v_z = 0$) than in the wings ($\pm v_z = \mathbf{v}$). Conversely, for a perfect **v**||**J** correlation, one would measure a Doppler profile with more intensity in the wings ($\pm v_z = \mathbf{v}$) than in the center ($v_z = 0$). Ideal Doppler profiles have been calculated in these two limits of **v**||**J** and **v**⊥**J** and are presented in Figure 7. We qualitatively conclude that the slight dip observed in the Doppler profiles is indicative of a **v**||**J** correlation. This result supports the model in which out of plane motion in the transition state, such as the torsional motion about the C−C bond, carries over into H_2 rotation as the photofragments separate.

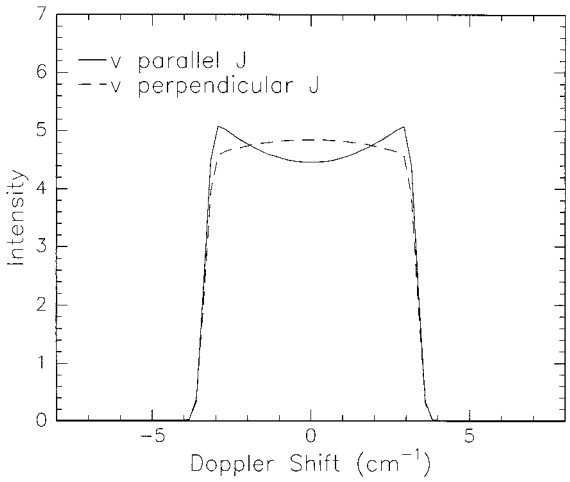

Figure 7. Calculated Doppler profiles.

The **v**−**J** correlations observed[52] for the CO products of glyoxal photodissociation at 440 nm indicate that **v**⊥**J** for CO. However, these measurements only extend down as low as $J = 21$, and likely refer to the dissociation channel leading to CH_2O + CO products and not the triple whammy channel. Nevertheless, in the planar dissociation model for the triple whammy channel, the CO molecules push off from one another (and the much lighter H_2) at an angle of 123° and would be expected to rotate in the plane of the dissociation with **v**⊥**J**.

E. Comparison of H_2 PHOFEX and Glyoxal Fluorescence Spectra. At first glance, the ratio of the unnormalized intensities of the H_2 PHOFEX and the glyoxal fluorescence spectra displayed in Figure 6 seems to indicate that the PHOFEX yield smoothly increases with vibrational energy in the S_1 excited state compared to the fluorescence yield. Quantum yields for fluorescence (Φ_F) and nonradiative decay processes (Φ_{NR}) have been measured[22] as a function of vibrational energy in S_1 glyoxal and do indeed show a drop off in fluorescence and an increase in nonradiative decay processes with energy. The experimental ratio of the H_2 PHOFEX signal intensity to that of the glyoxal fluorescence intensity can be related to the ratio of quantum yields for nonradiative and radiative decay as follows

$$\frac{I_{PHOFEX}}{I_{Fluor}} \propto \frac{\Phi_{NR}}{\Phi_F}\frac{C'}{C} \tag{5}$$

where C corrects Φ_F for the filter transmission curve, and C' accounts for the branching to the triple whammy channel among the other nonradiative decay (dissociation) channels included in Φ_{NR}. The C correction factors were calculated using the measured filter transmission curve and the relative intensities from dispersed fluorescence spectra obtained after excitation in each of the 4 main bands in Figure 6.[31,65−67] The resulting correction factors for the 4 bands differed by less than 5% and were subsequently ignored. The quantum yields Φ_F ($\Phi_{NR} = 1 - \Phi_F$) are listed in Table 2 along with the experimental ratios

TABLE 2: Comparison of Yields of TWC with S_1 Glyoxal Fluorescence as a Function of Vibrational Energy

mode excited	E_{vib} (S_1) (cm^{-1})	I_{PHOFEX}/I_{fluor}	Φ_F[a]	branching into TWC (C')[b]
0_0^0	0	0.98 ± 0.03	0.58	1.00 ± 0.03
7_0^2	464	2.12 ± 0.14	0.45	1.29 ± 0.09
5_0^1	509	1.91 ± 0.09	0.35	0.76 ± 0.04
8_0^1	735	2.56 ± 0.12	0.33	0.94 ± 0.04

[a] Reference 22. [b] C' values scaled to give unity for 0_0^0.

of the H_2 PHOFEX and glyoxal fluorescence intensities for four vibrational bands. With these quantities known, eq 5 may be rearranged to a form which is proportional to C', which describes how the yield of the H_2 state ($v = 1$, $J = 1$) in the triple whammy channel varies with vibrational energy in the initially excited S_1 glyoxal. The entries listed in Table 2 for C' do not show a smooth variation with vibrational energy but show a modest dependence on the vibrational mode excited. The largest yield corresponds to excitation in the 7_0^2 band, the out of plane torsional motion about the C−C bond. Such a motion would promote the trans to cis isomerization of glyoxal which is a necessary step on the way to the transition state and dissociation via the triple whammy channel as proposed by Osamura et al.[47] Excitation of the C−H wagging mode (8_0^1) is only slightly less efficient at promoting the yield of the triple whammy channel than excitation to the vibrationless mode (0_0^0). Excitation of the C−C−O bending mode (5_0^1), however, leads to a significantly reduced yield, perhaps due to vibrational motion which hampers the isomerization process or which prevents access to the minimum energy path along the TWC reaction coordinate.

F. Comparison to Photodissociation of Formaldehyde, Cyclohexadiene. All three channels in the photodissociation of glyoxal are examples of reactions which involve the breaking of several bonds and the formation of a new bond to form products. There has long been interest in determining whether such bonding changes occur sequentially or in a concerted fashion. Direct detection of intermediate species is one experimental method which clearly indicates that the reaction proceeds in a stepwise manner.[68] A less direct approach has been to measure the internal energy distributions of the several products and to compare the results with model predictions in the limiting cases of the stepwise or concerted mechanisms. A maximum entropy model using information theory, for example, has been developed and discussed with reference to photodissociation studies of acetone, carbon suboxide, and *s*-tetrazine.[69] A simpler model correlates the partitioning of energy among the degrees of freedom of the dissociation products with the structure of the parent molecule at its transition state. This model has been applied to reactions which are generally understood to follow a concerted dissociation such as the elimination of molecular H_2 in the photodissociation of alkenes.[70−72] It has also been discussed with reference to the dissociative electron impact ionization of simple alkanes and the resulting H_2^+ internal energy distributions.[73]

There are three characteristic features of this model of concerted molecular hydrogen elimination: (i) Translational energy release is dominant due to a substantial barrier in the exit channel of the potential energy surface and is determined by the C−H bond lengths at the transition state. (ii) The H−H separation in the transition state is usually larger than the equilibrium bond length in the ground vibrational level of free H_2, and leads to substantial vibrational excitation in the product H_2. (iii) Torque can be exerted on the departing H_2 only from an asymmetric transition state, or conversely, low rotational excitation in the H_2 product correlates with dissociation through a symmetric transition state.

The TWC in the dissociation of glyoxal compares favorably with other concerted H_2 elimination reactions for each of these model features. Table 3 summarizes the details relevant to such a model from photodissociation experiments involving formaldehyde[74,75] and cyclohexadiene,[70,76] and compares them with the TWC for glyoxal. In each case, the product average translational energy amounts to roughly two-thirds of the potential energy of the exit barrier. All three dissociations result in substantial vibration in the H_2 as indicated by the ratio of population in $v = 1$ to that in $v = 0$. For glyoxal, a lower limit was estimated based on the two-photon line strength factors[57] and considerations of the laser energies and the signal-to-noise ratios obtained in our experiments. With the large vibrational spacing of H_2, even a ratio of 11%, as for cyclohexadiene, corresponds to a very hot vibrational distribution with a vibrational temperature near 3000 K. Both glyoxal and cyclohexadiene dissociations have significantly less average energy in H_2 ($v = 1$) rotation than for formaldehyde. These results agree well with the ab initio calculations of symmetric transition states for glyoxal[47] and cyclohexadiene[77] and an asymmetric transition state for formaldehyde.[78] Notice that the **v**−**J** vector correlations also appear to follow this trend, that is, **v**||**J** occurs with dissociation from symmetric transition states (glyoxal and cyclohexadiene), and **v**⊥**J** occurs with the dissociation via an asymmetric transition state (formaldehyde).

V. Conclusion

Dissociation of glyoxal in the 440 nm region produces molecular hydrogen as a primary product, confirming that a fraction of the dissociation takes place via a channel that gives three photoproducts. The translational and internal energy distributions of the molecular hydrogen are consistent with calculations of the transition state for this dissociation.[47−49] It is a common observation that much of the energy difference along the reaction coordinate between the transition state and the products is released as translation, particularly if the transition state occurs late in the exit valley. The translational energy of the H_2 and CO products is about 46 kcal mol^{-1}, very close to the barrier energy for the triple whammy channel found experimentally[60] to be 47 kcal mol^{-1} and by ab initio theoretical calculations[49] to be 54.6 kcal mol^{-1}. The H_2 vibrational

TABLE 3: Comparison of Energy Partitioning for H_2 Elimination in the Photodissociation of Formaldehyde, Glyoxal, and Cyclohexadiene

	$CH_2O \rightarrow H_2 + CO$	$C_2H_2O_2 \rightarrow H_2 + 2CO$	$C_6H_8 \rightarrow H_2 + C_6H_6$
$E_{available}$ (kcal mol^{-1})	∼86	∼67	∼141
$E_{barrier}$ (kcal mol^{-1})	80	47	44
$E_{trans}/E_{available}$	>0.65	0.69	>0.5−0.8
H_2: $P(v = 1)/P(v = 0)$	∼1.7	>0.15	0.11
H_2 ($v = 1$): $\langle E_{rotn} \rangle$	1200 ± 120 cm^{-1}	725 ± 52 cm^{-1}	716 ± 110 cm^{-1}
H_2: **v**−**J** correlation	**v**⊥**J**	**v**||**J**	**v**||**J**
transition state	asymmetric	symmetric	symmetric
refs	74, 75, 78	this work, 47, 51	70, 76, 78

distribution is characterized by substantial population in $v = 1$, with some population in $v = 2$, whereas a Franck−Condon prediction of the H_2 vibrational energy based on the transition state geometry would also predict H_2 vibrational energy between $v = 1$ and $v = 2$. The H_2 rotational energy is found to be only about 3% of the total available energy, consistent with the planar geometry calculated for the transition state. Somewhat surprisingly, the small rotational excitation that we observe shows that the H_2 is rotating with its **J** vector parallel to its recoil velocity. Such excitation might reasonably be caused by out of plane torsion of the transition state structure, a motion that must be present in order for the *trans*-glyoxal to rotate into the cis conformation of the transition state. Further evidence that this torsional mode is important to the dissociation comes from the observation that the 7_0^2 excitation of this vibrational mode in S_1 glyoxal leads to an increased yield of H_2 when compared to excitation of the 0_0^0, 5_0^1, or 8_0^1 bands. Finally, the vector correlation and energy distributions we found for the glyoxal dissociation are consistent with those found for other concerted hydrogen elimination systems, $H_2CO \rightarrow H_2 + CO$,[74,75,78] and $C_6H_8 \rightarrow C_6H_5 + H_2$.[70,76,78]

Acknowledgment. It is a great pleasure to contribute this article to an issue of the *Journal of Physical Chemistry* honoring Kent Wilson. The photofragment translational spectroscopy experiments of Wilson and his group in the early 1970s inspired our own explorations of pump−probe photodissociation experiments, Doppler product spectroscopy, and product imaging. Wilson's curiosity and unique investigative abilities have been valuable guides and inspirations to the field of physical chemistry. We are also pleased to acknowledge informative discussions with Professor John Hepburn, Professor Luis Montero, and Professor Greg Sitz, and we are grateful to Professor Remy Jost who provided us with dispersed fluorescence spectra of glyoxal. Darcy Peterka assisted in some of the experimental work described here. This project was supported by the National Science Foundation under Grant CHE-9531705. W.K. was supported by an NSERC postdoctoral fellowship.

References and Notes

(1) Paldus, J.; Ramsay, D. A. *Can. J. Phys.* **1967**, *45*, 1389.
(2) Agar, D. M.; Bair, E. J.; Birss, F. W.; Borrell, P.; Chen, P. C.; Currie, G. N.; McHugh, A. J.; Orr, B. J.; Ramsay, D. A.; Roncin, J. Y. *Can. J. Phys.* **1971**, *49*, 323−327.
(3) Currie, G. N.; Ramsay, D. A. *Can. J. Phys.* **1971**, *49*, 317−322.
(4) Holzer, W.; Ramsay, D. A. *Can. J. Phys.* **1970**, *48*, 1759−1765.
(5) Birss, F. W.; Brown, J. M.; Cole, A. R. H.; Lofthus, A.; Krishnamachari, S. L. N. G.; Osborne, G. A.; Paldus, J.; Ramsay, D. A.; Watmann, L. *Can. J. Phys.* **1970**, *48*, 1230−1241.
(6) Coetz, W.; McHugh, A. J.; Ramsay, D. A. *Can. J. Phys.* **1970**, *48*, 1−5.
(7) Cole, A. R. H.; Braund, D. B.; Ramsay, D. A. *8th Aust. Spectrosc. Conf. Abstr.* **1971**, 121.
(8) Dong, R. Y.; Ramsay, D. A. *Can. J. Phys.* **1973**, *51*, 1491−1496.
(9) Dong, R. Y.; Ramsay, D. A. *Can. J. Phys.* **1973**, *51*, 1463−1465.
(10) Ramsay, D. A.; Zauli, C. *Acta Phys. Acad. Sci. Hung.* **1974**, *35*, 79−83.
(11) Birss, F. W.; Braund, D. B.; Cole, A. R. H.; Engleman, R., Jr.; Green, A.; Japar, S. M.; Nanes, R.; Orr, B. J.; Ramsay, D. A.; Szyszka, J. *Can. J. Phys.* **1977**, *55*, 390−395.
(12) Ramsay, D. A.; Vervloet, M.; Vanhorenbeke, F.; Godefroid, M.; Herman, M. *J. Mol. Spectrosc.* **1991**, *149*, 348−355.
(13) Lombardi, M.; Jost, R.; Michel, C.; Tramer, A. *Chem. Phys.* **1980**, *46*, 273−279.
(14) Lombardi, M.; Jost, R.; Michel, C.; Tramer, A. *Chem. Phys.* **1981**, *57*, 341−353.
(15) Lombardi, M.; Jost, R.; Michel, C.; Tramer, A. *Chem. Phys.* **1981**, *57*, 355−363.
(16) Jost, R.; Lombardi, M.; Michel, C.; Tramer, A. *Nuovo Cimento B (Italy), Nuovo Cimento B* **1981**, *63B*, 228−232.
(17) Pebay-Peyroula, E.; Jost, R.; Lombardi, M.; Pique, J. P. *Chem. Phys.* **1986**, *106*, 243−257.
(18) Anderson, L. G.; Parmenter, C. S.; Poland, H. M.; Rau, J. D. *Chem. Phys. Lett.* **1971**, *8*, 232−234.
(19) Holtzclaw, K. W.; Moss, D. B.; Parmenter, C. S.; Loge, G. W. *J. Phys. Chem.* **1983**, *87*, 4495−4503.
(20) Sorokin, N. I.; Bazhin, N. M.; Eremenchuk, G. G. *Chem. Phys. Lett.* **1983**, *99*, 181−185.
(21) Kato, H.; Sawa, K.; Kuwano, H.; Kasahara, S.; Baba, M.; Nagakura, S.; Oonishi, T.; Nishizawa, K. *J. Chem. Phys.* **1998**, *109*, 4798−4806.
(22) MacDonald, B. G.; Lee, E. K. C. *J. Chem. Phys.* **1979**, *71*, 5049−5052.
(23) Naaman, R.; Lubman, D. M.; Zare, R. N. *J. Chem. Phys.* **1979**, *71*, 4192−4200.
(24) Tuazon, E. C.; MacLeod, H.; Atkinson, R.; Carter, W. P. L. *Environ. Sci. Technol.* **1986**, *20*, 383−387.
(25) Finlayson-Pitts, B. J.; Pitts, J. J. N. *Atmospheric Chemistry: Fundamentals and Experimental Techniques*; John Wiley & Sons: New York, 1986.
(26) Hucknall, D. J. *Chemistry of Hydrocarbon Combustion*; Chapman and Hall: London, 1985.
(27) Parmenter, C. S.; Seaver, M. *J. Chem. Phys.* **1979**, *70*, 5458−5462.
(28) Butz, K. W.; Du, H.; Krajnovich, D. J.; Parmenter, C. S. *J. Chem. Phys.* **1987**, *87*, 3699−3700.
(29) Butz, K. W.; Du, H.; Krajnovich, D. J.; Parmenter, C. S. *J. Chem. Phys.* **1988**, *89*, 4680−4691.
(30) Butz, K. W.; Krajnovich, D. J.; Parmenter, C. S. *J. Chem. Phys.* **1990**, *93*, 1557−1567.
(31) Gilbert, B. D.; Parmenter, C. S.; Krajnovich, D. J. *J. Chem. Phys.* **1994**, *101*, 7423−7439.
(32) Gilbert, B. D.; Parmenter, C. S.; Krajnovich, D. J. *J. Phys. Chem.* **1994**, *98*, 7116−7122.
(33) Gilbert, B. D.; Parmenter, C. *S. J. Chem. Phys.* **1994**, *101*, 7440−7450.
(34) Parmenter, C. S.; Clegg, S. M.; Krajnovich, D. J.; Lu, S.-P. *Proc. Natl. Acad. Sci. U.S.A.* **1997**, *94*, 8387−8392.
(35) Clegg, S. M.; Gilbert, B. D.; Lu, S.-P.; Parmenter, C. S. *ACS Symp. Ser.* **1997**, *678*, 237−250.
(36) Clegg, S. M.; Burrill, A. B.; Parmenter, C. S. *J. Phys. Chem. A* **1998**, *102*, 8477−8485.
(37) Weida, M. J.; Parmenter, C. S. *J. Phys. Chem. A* **1997**, *101*, 9594−9602.
(38) Jouvet, C.; Soep, B. *J. Chem. Phys.* **1981**, *75*, 1661−1666.
(39) Zhu, L.; Kellis, D.; Ding, C.-F.; Frye, D.; Arias, P.; Dai, H. L. *Chem. Phys. Lett.* **1996**, *257*, 487−491.
(40) Sulkes, M.; Jouvet, C.; Rice, S. A. *Chem. Phys. Lett.* **1982**, *93*, 1−4.
(41) Yamanouchi, K.; Yamada, H.; Tsuchiya, S.; Spangler, L. H.; Pratt, D. W.; Malstrom, R. A.; Photos, E.; Atkinson, G. H. *Chem. Phys. Lett.* **1986**, *132*, 361−364.
(42) Kim, H. L.; Reid, S.; McDonald, J. D.; Frye, D.; Liou, H. T.; Dai, H. L. *Chem. Phys. Lett.* **1987**, *139*, 525−527.
(43) Loge, G. W.; Parmenter, C. S.; Rordorf, B. F. *Chem. Phys. Lett.* **1980**, *74*, 309−313.
(44) Loge, G. W.; Parmenter, C. S. *J. Phys. Chem.* **1981**, *85*, 1653−1662.
(45) Loge, G. W.; Parmenter, C. S. *J. Chem. Phys.* **1981**, *74*, 29−35.
(46) Parmenter, C. S. *J. Chem. Phys.* **1964**, *41*, 658.
(47) Osamura, Y.; Schaefer, H. F., III; Dupuis, M.; Lester, W. A., Jr. *J. Chem. Phys.* **1981**, *75*, 5828−5836.
(48) Osamura, Y.; Schaefer, H. F., III. *J. Chem. Phys* **1981**, *74*, 4576−4580.
(49) Scuseria, G. E.; Schaefer, H. F., III. *J. Am. Chem. Soc.* **1989**, *111*, 7761−7765.
(50) Montero, L., private communication.
(51) Hepburn, J. W.; Buss, R. J.; Butler, L. J.; Lee, Y. T. *J. Phys. Chem.* **1983**, *87*, 3638−3641.
(52) Burak, I.; Hepburn, J. W.; Sivakumar, N.; Hall, G. E.; Chawla, G.; Houston, P. L. *J. Chem. Phys.* **1987**, *86*, 1258−1268.
(53) Further details of this experiment can be found in the following: Dobeck, L. M. Photodissociation Dynamics of Glyoxal: Evidence for the Channel Producing H_2 + CO. Ph.D. Thesis, Cornell University, 1999.
(54) Proch, D.; Trickl, T. *Rev. Sci. Instrum.* **1989**, *60*, 713−716.
(55) Vrakking, M. J. J.; Bracker, A. S.; Suzuki, T.; Lee, Y. T. *Rev. Sci. Instrum.* **1993**, *64*, 645−652.
(56) Marinero, E. E.; Vasudev, R.; Zare, R. N. *J. Chem. Phys.* **1983**, *78*, 692.
(57) Huo, W. M.; Rinnen, K.-D.; Zare, R. N. *J. Chem. Phys.* **1991**, *95*, 205.
(58) Pebay-Peyroula, E.; Jost, R. *J. Mol. Spectrosc.* **1987**, *121*, 177.
(59) Weissman, S.; Vanderslice, J. T.; Battino, R. *J. Chem. Phys.* **1963**, *39*, 2226.

(60) Saito, K.; Kakumoto, T.; Murakami, I. *J. Phys. Chem.* **1984**, *88*, 1182.
(61) Butz, K. W.; Johnson, J. R.; Krajnovich, D. J.; Parmenter, C. S. *J. Chem. Phys.* **1987**, *86*, 5923.
(62) Kummel, A. C.; Sitz, G. O.; Zare, R. N. *J. Chem. Phys.* **1986**, *85*, 6874; **1988**, *88*, 6707.
(63) Hanisco, T. F.; Kummel, A. C. *J. Phys. Chem.* **1991**, *95*, 8565; **1992**, *96*, 2982.
(64) Note: the value of $P_0^{(2)}/P_0^{(0)} = 0.4$ suggests that the Q branch transitions are comparable to S branch transitions in the magnitude of the polarization dependence. This is inconsistent with unpublished observations of G. O. Sitz and co-workers.
(65) Atkinson, G. H.; Malstrom, R. A.; McIlwain, M. E. *J. Mol. Spectrosc.* **1979**, *76*, 164−181.
(66) Pebay-Peyroula, E.; Delon, A.; Jost, R. *J. Mol. Spectrosc.* **1988**, *132*, 123.
(67) Butz, K. W.; Du, H.; Krajnovich, D. J.; Parmenter, C. S. *J. Chem. Phys.* **1988**, *89*, 4680.
(68) Kim, S. K.; Pedersen, S.; Zewail, A. H. *J. Chem. Phys.* **1995**, *103*, 477.
(69) Strauss, C. E. M.; Houston, P. L. *J. Phys. Chem.* **1990**, *94*, 8751.
(70) Zhao, X.; Continetti, R. E.; Yokojama, A.; Hintsa, E. J.; Lee, Y. T. *J. Chem. Phys.* **1989**, *91*, 4118.
(71) Venkataraman, B. K.; Valentini, J. J. *Chem. Phys. Lett.* **1992**, *194*, 191.
(72) Cromwell, E. F.; Stolow, A.; Vrakking, M. J. J.; Lee, Y. T. *J. Chem. Phys.* **1992**, *97*, 4029.
(73) Beijersbergen, J. H. M.; van der Zande, W. J.; Kistemaker, P. G.; Los, J. *J. Phys. Chem.* **1993**, *97*, 11180.
(74) Butenhoff, T. J.; Carleton, K. L.; Moore, C. B. *J. Chem. Phys.* **1990**, *92*, 377.
(75) Carleton, K. L.; Butenhoff, T. J.; Moore, C. B. *J. Chem. Phys.* **1990**, *93*, 3907.
(76) Cromwell, E. F.; Liu, D.-J.; Vrakking, M. J. J.; Kung, A. H.; Lee, Y. T. *J. Chem. Phys.* **1991**, *95*, 297.
(77) Rico, R. J.; Page, M.; Doubleday, C., Jr. *J. Am. Chem. Soc.* **1992**, *114*, 1131.
(78) Goddard, J. D.; Yamaguchi, Y.; Schaeffer, H. F., III. *J. Chem. Phys.* **1981**, *75*, 3459.